HHS Public Access

Author manuscript

Oncogene. Author manuscript; available in PMC 2019 May 06.

Published in final edited form as:

Oncogene. 2019 March ; 38(12): 2056–2075. doi:10.1038/s41388-018-0543-2.

ACVR1C/SMAD2 signaling promotes invasion and growth in retinoblastoma

Laura Asnaghi[1], **David T. White**[2], **Nolan Key**[1], **Joshua Choi**[1], **Alka Mahale**[4], **Hind Alkatan**[4,#], **Deepak P. Edward**[2,4,6], **Sahar M. Elkhamary**[4,5], **Saleh Al-Mesfer**[4], **Azza Maktabi**[4], **Christopher G. Hurtado**[2], **Grace Y. Lee**[2], **Angel M. Carcaboso**[7], **Jeff S. Mumm**[2], **Leen Abu Safieh**[4,*], and **Charles G. Eberhart**[1,2,3,*]

[1]Department of Pathology, [2]Ophthalmology, and [3]Oncology, Johns Hopkins University, School of Medicine, Baltimore, Maryland, USA [4]King Khaled Eye Specialist Hospital, Riyadh, Saudi Arabia [5]Department of Diagnostic Radiology, Mansoura Faculty of Medicine, Mansoura, Egypt, [6]University of Illinois Eye and Ear Infirmary, Chicago, Illinois [7]Institut de Recerca Sant Joan de Deu, Barcelona, Spain [#] Current affiliation: Department of Ophthalmology, College of Medicine, King Saud University, Riyadh, Saudi Arabia.

Abstract

Retinoblastoma is the most common intraocular cancer in children. While the primary tumor can often be treated by local or systemic chemotherapy, metastatic dissemination is generally resistant to therapy and remains a leading cause of pediatric cancer death in much of the world. In order to identify new therapeutic targets in aggressive tumors, we sequenced RNA transcripts in five snap frozen retinoblastomas which invaded the optic nerve and five which did not. A three-fold increase was noted in mRNA levels of ACVR1C/ALK7, a type I receptor of the TGF-β family, in invasive retinoblastomas, while downregulation of DACT2 and LEFTY2, negative modulators of the ACVR1C signaling, was observed in most invasive tumors. A two- to three-fold increase in ACVR1C mRNA was also found in invasive WERI Rb1 and Y79 cells as compared to non-invasive cells *in vitro*. Transcripts of ACVR1C receptor and its ligands (Nodal, Activin A/B, and GDF3) were expressed in six retinoblastoma lines, and evidence of downstream SMAD2 signaling was present in all these lines. Pharmacological inhibition of ACVR1C signaling using SB505124, or genetic downregulation of the receptor using shRNA potently suppressed invasion, growth, survival, and reduced the protein levels of the mesenchymal markers ZEB1 and Snail. The inhibitory effects on invasion, growth, and proliferation were recapitulated by knocking down SMAD2, but not SMAD3. Finally, in an orthotopic zebrafish model of retinoblastoma, a 55% decrease in tumor spread was noted (p=0.0026) when larvae were treated with 3 μM of SB505124, as compared to DMSO. Similarly, knockdown of ACVR1C in injected tumor cells using shRNA

[*]Corresponding Authors: Charles G. Eberhart, M.D., Ph.D.: Department of Pathology, Johns Hopkins University, School of Medicine, Smith Building, 400 N. Broadway Avenue, Baltimore, MD, 21287. Phone: 410-502-5185; fax: 410-955-9777; ceberha@jhmi.edu; or Leen Abu Safieh, Ph.D: King Khaled Eye Specialist Hospital, Riyadh, Saudi Arabia. Phone: +966-1-4821234; leensafieh@yahoo.co.uk.

Disclosure/Conflict of Interest: The Authors declare no conflict of interest.

also resulted in a 54% reduction in tumor dissemination in the zebrafish eye as compared to scrambled shRNA control (p=0.0005). Our data support a role for the ACVR1C/SMAD2 pathway in promoting invasion and growth of retinoblastoma.

Keywords

Retinoblastoma; RNA-seq; invasion; ACVR1C; SMAD; Nodal

INTRODUCTION

Retinoblastoma is the most common pediatric intraocular cancer, affecting approximately 300 children per year in the United States and causing approximately 4,000 deaths annually worldwide (1). In Saudi Arabia, according to the Cancer Incidence Report 2014, it accounts for 3.3% of childhood cancers and is listed among the top ten most common cancers in Saudi children at 5.7% among girls and 1.5% among boys. While the primary tumor can often be successfully treated by local and/or systemic chemotherapy, extraocular dissemination through the optic nerve into the central nervous system (CNS) or through the choroid into the bloodstream, represents a serious clinical complication. Metastatic progression occurs in cases which are particularly aggressive or not treated promptly, and usually appears within the first year after diagnosis (1). Metastases in the CNS or in distant organs, such as bone and bone marrow, are resistant to current therapies and generally fatal (2,3). CNS involvement is the most common complication, with nearly 100% mortality (1). The molecular factors driving metastatic spread are not well understood, thus there is an urgent need to elucidate the molecular drivers responsible for retinoblastoma invasion into the optic nerve and other sites, in order to establish new therapeutic targets.

Here we show that Activin A receptor type 1C (ACVR1C), also known as Activin-like kinase receptor 7 (ALK7), as well as downstream signaling by homologues of the Drosophila protein, mothers against decapentaplegic (Mad) and the Caenorhabditis elegans protein Sma, family member 2 (SMAD2) plays an important role in promoting retinoblastoma dissemination. ACVR1C/ALK7 is a type I receptor of the TGF-β (transforming growth factor-beta) family, which binds Nodal, Activin A/B, and GDF3 (growth and differentiation factor 3), and is predominantly expressed in the central nervous system, colon and pancreas (4).

Members of the TGF-β superfamily include TGF-β1, bone morphogenic protein (BMP), Nodal, Activin A/B and GDF, which are known to control many physiological processes, including proliferation, differentiation, wound healing, and immune responses (5). TGF-β signaling regulates tumor growth and invasion in a number of contexts (6–8). Nodal and Activin cytokines both bind to ACVR1B (ALK4) and ACVR1C (ALK7) receptors, which have intrinsic serine/threonine kinase activities in their cytoplasmic domains, inducing phosphorylation and activation of the SMAD2/3/4 complex, which translocates into the nucleus where it binds SMAD-binding elements (SBE) to activate gene transcription (9). Activin, Nodal and TGF-β ligands share the downstream effectors SMAD2 and SMAD3, thus they can have similar functions, but they often display distinct tissue expression

patterns. Aberrant re-expression of Nodal, Activin, and TGF-β signaling has a prominent role in tumorigenesis and metastasis for melanoma, breast, prostate, and pancreatic cancers, where levels of Nodal are directly proportional to tumor grade (9–11). Activin A also promotes anchorage-independent growth, epithelial-to-mesenchymal transition (EMT), invasion and stemness of breast cancer cells by SMAD-dependent signaling (12). Prior studies have thus established a role for Nodal/Activin/TGF-β pathway in promoting a stem/progenitor like phenotype in several tissues, and inducing tumor growth and metastasis. Here we found that inhibition of this signaling potently suppressed a metastatic phenotype in retinoblastoma cells, both *in vitro* and *in vivo*.

RESULTS

Next generation RNA sequencing data

Gene expression differences between five non-invasive (cases 1–5) and five invasive (cases 6–10) retinoblastoma specimens, whose clinical characteristics are summarized in Table S1, were quantified. Optic nerve invasion was identified by Magnetic Resonance Imaging (MRI) and confirmed by microscopic analysis of resected tumors. Representative MRI images with either no invasion, limited retrolaminar invasion or extensive dissemination in the optic nerve are shown in Figure 1a, b, and c, respectively. Using RNA sequencing, we found 153 genes whose mean expression was altered by more than 2-fold in the invasive cohort: 33 were upregulated and 120 were downregulated. The genes which showed an increase of 2-fold or more are listed in Table 1 and Figure S1. The most upregulated gene in the invasive cohort was *ADCYAP1* (*adenylate cyclase activating polypeptide 1*), whose expression increased almost 60 fold. The *ADCYAP1* gene product (PACAP, pituitary adenylate cyclase activating polypeptide) is normally expressed in the central nervous system, including retinal ganglion cells, and in most peripheral organs (13). The most upregulated genes previously associated with tumor spread included *DLX6* (*distal-less homeobox* 6), associated with metastatic progression in breast cancer (14), and *MMP12* (*matrix metallopeptidase*), involved in promoting invasion in lung and nasopharyngeal carcinoma (15,16). In addition we found two-fold upregulation of *IQGAP3* (*IQ motif containing GTPase activating protein 3*), an effector of Rac/Cdc42, which promotes cell migration/invasion by interacting with small GTPase proteins (17,18).

ACVR1C (ALK7) levels were induced in all cases of invasive retinoblastoma (Figure 1d). ACVR1C is a type I receptor of the TGF-β family, which binds Nodal, Activin A/B, and GDF3 (9). Furthermore, *DACT2* (*dishevelled binding antagonist of beta catenin 2*), a negative regulator of the Nodal/TGF-β signaling (19), was downregulated more than 28-fold on average in the invasive cohort, while *LEFTY2* (*left-right determination factor 2*), a natural inhibitor of the Nodal/TGF-β pathway (20), was reduced about 10-fold on average in the invasive group (Figure 1d). ACVR1C was also induced in invasive WERI Rb1 and Y79 retinoblastoma cells *in vitro*. In cells that migrated through a filter pre-coated with Matrigel, ACVR1C mRNA levels were two-fold higher in both WERI Rb1 ($p=0.01$) and Y79 cells ($p=0.0027$) as compared to those which did not move from the insert (Figure 1e).

Several reductions in gene expression were also identified in invasive retinoblastomas (Table 2, Figure S1). The most downregulated gene was *CRABP1* (*cellular retinoic acid binding*

protein 1), which regulates differentiation and is considered a candidate tumor suppressor in esophageal carcinoma (21). Other genes whose expression was significantly reduced in the invasive tumors include: *GFAP* (*glial fibrillary acidic protein*) and *RHO* (*rhodopsin*), both markers of cell differentiation in retinoblastoma cells (22), and *NGFR* (*nerve growth factor receptor*). In addition, *DACT2*, a negative regulator of the Nodal and WNT signaling (19), was reduced 28-fold in the invasive cohort.

Components of the ACVR1C/SMAD2 pathway are expressed in retinoblastoma cells

The ACVR1C receptor as well as its ligands, Nodal, Activin A/B, and GDF3, were expressed at the mRNA level in six retinoblastoma-derived cell lines: WERI Rb1, Y79 and RB143 (patient-derived primary lines which grow in the presence of serum), HSJD-RBT-1 and HSJD-RBT-2 (patient-derived primary lines which grow in serum-free medium), and HSJD-RBVS-10, a serum-free line derived from tumor seeding in the vitreous (Figure 2a-e). The ligands and receptors expressed in the retinoblastoma cells appear to activate downstream SMAD signaling, with phosphorylation of SMAD2, the main downstream effector of Nodal/TGF-β pathway, in all retinoblastoma lines analyzed (Figure 2f). In contrast, SMAD3 was expressed only in WERI Rb1 and Y79, but no phosphorylation was detected in any retinoblastoma line (Figure 2f). We also found elevated protein expression of Nodal and GDF3 ligands in HSJD-RBT-2, WERI Rb1 and Y79, as opposed to HSJD-RBVS-10 and RB143, which expressed lower protein levels of these ligands (Figure 2f). Stimulated PANC-1 cells were used as positive controls for these antibodies (Figure S2). Nodal was expressed mostly in the cytosol and cell membrane in WERI Rb1 and Y79, as determined by immunofluorescence (Figure 2g).

Pharmacological blockade of the ACVR1C/SMAD2 pathway represses growth and invasion in retinoblastoma cells

Pharmacological inhibition of the ACVR1C receptor using SB505124, a selective inhibitor of ALK4/5/7 receptors (23), significantly reduced growth (Figure 3a, c, e) and invasion (Figure 3b, d, f) of cultured retinoblastoma cells in a dose-dependent manner. In WERI Rb1 cells, growth was potently suppressed, starting at 2 μM after 3, 5, and 7 days of treatment (Figure 3a). Y79 growth was almost completely suppressed at concentrations ≥ 1 μM (Figure 3c), while HSJD-RBVS-10 cells were somewhat less responsive to SB505124-mediated growth inhibition (Figure 3e). Nevertheless, SB505124 potently suppressed invasion of all three lines in a dose-dependent manner, as found by transwell invasion assay, with more than 70% inhibition in the ability of the cells to invade through a Matrigel-coated filter at concentrations ≥ 3 μM (Figure 3b, d, f).

The effects on growth and invasion were paralleled by a dose-dependent inhibition in SMAD2 phosphorylation upon treatment with SB505124 at 0.5, 1, 2, 3, 4, 8 μM for 4 days (Figure 4a-c). SB505124 did not modify phosphorylation of SMAD3, which was minimal in these lines. However, we observed a dose-dependent decrease in the total levels of SMAD3 in WERI Rb1 and Y79 (Figure 4a-b, bottom panel).

Interestingly, the reduction in invasion also correlated with a dose-dependent decrease in protein levels of the epithelial-to-mesenchymal transition markers ZEB1 (*zinc finger E-box*

binding homeobox 1) and Snail, as found by Western blot in all three retinoblastoma lines examined (Figure 4a-c).

Some of the reduced growth in viable cell mass was due to decreased survival of cells, as treatment with SB505124 also induced a dose-dependent increase in cleaved PARP, a marker of late apoptosis (Figure 4a-c). The induction of apoptosis was also confirmed by cleaved caspase-3 assay in WERI Rb1, Y79 (Figure 4d, e) and in HSJD-RBVS-10 (data not shown). These findings indicate that the ACVR1C/SMAD2 pathway promotes growth, survival, and invasive properties in retinoblastoma cells.

Genetic downregulation of the ACVR1C/SMAD2 pathway inhibits invasion and proliferation in Y79 cells

To further establish the role of the ACVR1C receptor in promoting invasion and growth of retinoblastoma, we genetically inhibited its expression by short hairpin RNA (shRNA). Two target sequences were effective in reducing ACVR1C mRNA levels by more than 80% ($p=0.007$, Figure 5a). This reduction was accompanied by approximately 70% inhibition in invasion, as determined by transwell invasion assay (Figure 5b), with a significant downregulation of mRNA and protein levels of Snail (Figure 5c, d), and in the decreased protein levels of ZEB1 (Figure 5d). SMAD2 phosphorylation was also reduced in cells expressing ACVR1C shRNA as compared to scrambled shRNA, supporting this downstream effector as a potential mediator of ACVR1C signaling in retinoblastoma. Y79-GFP cells expressing ACVR1C shRNA showed high levels of cleaved PARP as compared to cells transduced with scrambled shRNA or parental line (Figure 5d) indicating reduced survival. We then assessed the ability of these cells to grow and proliferate, by performing respectively CCK-8 and Ki67 assays, respectively. Growth was potently reduced in ACVR1C shRNA-expressing cells as compared to scrambled shRNA (Figure 5e). We also found 40 to 50% reduction in the percentage of Ki67-positive cells using both shRNAs as compared to scrambled control, confirming a decrease in proliferation upon reduction of ACVR1C expression ($p<0.0001$, Figure 5f).

To address the role of SMAD2 and SMAD3 in mediating the downstream effects of ACVR1C, we repressed the expression of SMAD2 or SMAD3 by shRNA in Y79 cells. We used three target sequences for each gene, and found that all of them effectively reduced the protein levels of SMAD2 (Figure S3a) and SMAD3 (Figure S4a). This reduction was paralleled by about 80% decrease in invasion, when cells where transduced with shSMAD2 (Figure S3b), but no difference was observed when SMAD3 was knocked down (Figure S4b). Likewise, proliferation and growth were significantly reduced when SMAD2 expression was inhibited (Figure S3c,d), as opposed to SMAD3 downregulation, which did not inhibit either replication or growth, as found by Ki67 and CCK-8 assay, respectively (Figure S4c,d). Since we observed that only the knock-down of SMAD2, but not SMAD3, recapitulated the inhibitory effects on invasion, growth, and proliferation, associated with lowered levels of ACVR1C receptor, we believe that the pathway induced by ACVR1C signaling is mediated downstream mostly by SMAD2.

Treatment with recombinant Nodal does not affect invasion, proliferation and growth in WERI Rb1 and Y79 cells

To address the role of ACVR1C ligands in regulating growth and invasion in retinoblastoma, we stimulated WERI Rb1 and Y79 cells with human recombinant Nodal. Surprisingly, we did not observe any further increase in SMAD2 phosphorylation upon treatment with Nodal at 100, 300, 500 ng/mL, for 2 hours in either line (Figure S5a). Similarly, invasion, proliferation and growth were not significantly modified by Nodal treatment in these cells (Figure S5b-d). Thus the relatively high levels of Nodal present in WERI Rb1 and Y79 at steady state (Fig. 2f-g) may already maximally induce tumorigenic effects.

Pharmacological and genetic inhibition of the ACVR1C/SMAD2 signaling reduces retinoblastoma cell dissemination *in vivo* in Zebrafish

Y79 cells, labelled with GFP, were injected intravitreally in the zebrafish eye at 2 days post-fertilization (dpf). Zebrafish larvae (n=12) were then treated with DMSO or 3 μM of SB505124 for 4 days. Cells were monitored longitudinally by confocal microscopy at 1 and 4 days post-injection (dpi). No significant increase in cell number was seen over this time period, however we observed that the Y79-GFP cells spread from the initial injection site and some had migrated outside the eye at 4 dpi. Minimum bounding spheres (MBS) were used to outline the extent of tumor dissemination, and are highlighted in red (Figure 6a). A significant increase in retinoblastoma cell spread over time was observed in DMSO control larvae ($p=0.0082$), but not in those treated with SB505124 ($p=0.59$; Figure 6b). Because no significant change in cell number was identified over this time, the 55% reduction in MBS diameter fold change when larvae were treated with 3 μM of SB505124 for 4 days as compared to DMSO was most likely due to effects on tumor invasion rather than proliferation or survival ($p=0.0026$; Figure 6c).

Genetic inhibition of the pathway showed similar results. Y79-GFP cells expressing ACVR1C shRNA or scrambled shRNA were injected intravitreally in zebrafish larvae and monitored longitudinally by confocal microscopy at 1 and 4 dpi (Figure S6a). We found a significant increase in cell spread in the cohort injected with Y79-GFP expressing scrambled shRNA ($p=5.66\times10^{-5}$) but not in those with ACVR1C shRNA ($p=0.29$) as measured by MBS diameter (Figure S6b). A significant 54% reduction in MBS diameter fold-change, indicative of reduction in tumor dissemination, was observed in the cohort injected with Y79-GFP cells expressing ACVR1C shRNA, as compared to scrambled shRNA ($p=0.0005$; Figure S6c). These *in vivo* findings further support the concept that targeting the ACVR1C/SMAD2 pathway may be effective in treating retinoblastoma invasion.

DISCUSSION

Retinoblastoma causes significant morbidity including loss of vision, and when metastatic usually leads to death, as metastases are generally resistant to current chemotherapeutic regimens (24,25). Although extraocular retinoblastoma is rare in the Western countries, it is more frequent in the developing world. In low-income countries of Asia and Africa, extraocular disease is present in 20% to 50% of all retinoblastoma cases (26,27) and is almost always fatal. Here we focused on the role of ACVR1C/SMAD2 signaling in

promoting invasion and growth in retinoblastoma, as we found that the mRNA levels of *ACVR1C* (*ALK7*), a type I serine/threonine kinase receptor of the TGF-β family, were increased in all invasive retinoblastoma specimens that we have analyzed by next generation RNA sequencing. Downregulation of natural inhibitors of ACVR1C/SMAD2 signaling, such as *DACT2* and *LEFTY2*, was also observed in most of the invasive cases.

The ACVR1C receptor binds to members of the TGF-β superfamily, such as Nodal, Activin A/B, and GDF3, leading to activation, through serine-threonine phosphorylation, of SMAD2 and SMAD3 downstream effectors. The cofactor SMAD4 combines with the activated form of SMAD2/3, forming a complex which translocates in the nucleus, activating gene transcription (5,9). Activin and Nodal are known to maintain pluripotency in human embryonic stem cells by controlling Nanog expression, and disruption of these pathways results in cell differentiation (28).

Growing evidence has also shown that TGF-β, Nodal and Activin signaling regulates tumor progression and metastasis (29). Nodal is highly expressed in metastatic melanoma, but not in normal melanocytes or noninvasive melanoma (30), and antibodies against Nodal have been shown to induce apoptosis in melanoma cells (31). Nodal is also expressed in breast cancer in correlation with disease progression and is required to induce, through ERK signaling, a tumorigenic phenotype in triple-negative breast cancers (11). Conversely, overexpression of *ACVR1C* has been associated with decreased growth and adhesion in breast cancer (32), while downregulation of this receptor has been linked to poor prognosis and metastasis in pancreatic adenocarcinoma (9). However, activating mutations in a receptor of the same family, ACVR1 (ALK2), specific for bone morphogenetic protein (BMP), are present in 33% of Diffuse Intrinsic Pontine Glioma (DIPG), a highly invasive pediatric brain tumor (33).

Activin, another ligand of ACVR1C receptor, also plays a key role in cancer biology. It is upregulated in breast cancer, as indicated by the significant increase in the levels of Activin A and phospho-SMAD2–3 in advanced breast cancer as compared to normal tissues (12). In addition, prior studies have linked Nodal/Activin signaling to an invasive phenotype in several human cancers. In breast cancer, Nodal promotes EMT via SMAD2/3 pathway, by inducing *Snail* and *Slug* gene transcription (34). In esophageal carcinoma, Activin A is associated with invasion and poor prognosis, through induction of N-cadherin (35).

We directly investigated the functional role of ACVR1C/SMAD2 in the regulation of invasion and overall growth in retinoblastoma lines derived from primary tumors (WERI Rb1 and Y79), or vitreous seeds (HSJD-RBVS-10), using both a pharmacological and a genetic approach to suppress the pathway. We found that inhibition of ACVR1C/SMAD2 pathway, using SB505124, a selective inhibitor of ALK4/5/7 receptors (23), or downregulation of ACVR1C or SMAD2 by shRNAs, strongly suppressed the invasive properties of retinoblastoma cells both *in vitro* and *in vivo*. In parallel, we observed reductions in overall growth as well as proliferation, indicating a role for the ACVR1C/SMAD2 pathway in sustaining multiple aspects of retinoblastoma pathobiology. Importantly, using an orthotopic model of retinoblastoma invasion in zebrafish, we

confirmed *in vivo* that blockade of the ACVR1C-mediated pathway produced more than 50% inhibition in the ability of Y79-GFP cells to disseminate.

In contrast, SMAD3 was not phosphorylated in the retinoblastoma lines that we analyzed, and its downregulation did not modify invasion, growth or proliferation in Y79 cells. It is not clear why SMAD2, but not SMAD3, is activated in these tumors. Stimulation of WERI Rb1 and Y79 cells with exogenous TGF-β1 ligand did not result in SMAD3 phosphorylation (data not shown). Analysis of 36 cases of retinoblastoma included in the Pediatric Pan-Cancer group (DKFZ - German Cancer Consortium, 2017) using CBioPortal (http://www.cbioportal.org) did not identify alterations in *SMAD3* or *ACVR1C*, which might have modulated activation of SMAD3. However, it has been shown in some non-neoplastic settings that SMAD2 and SMAD3 can be differentially activated by TGF-β family ligands (36,37). The issue of the selective phosphorylation of SMAD2 but not SMAD3 by the ACVR1C-mediated pathway in retinoblastoma cells is intriguing and worthy of further investigation.

We believe that the inhibitory effects on invasion may be mediated at least in part by the downregulation of EMT factors, such as ZEB1 and Snail, as we found a dramatic reduction in their protein levels upon pharmacological or genetic blockade of ACVR1C-mediated signaling. It is known that these EMT factors promote invasion and metastasis in other tumor models (38) and their expression is regulated, among other mechanisms, by SMAD2 signaling (34,39,40). Previous studies have also shown that inactivation of RB protein contributes to tumor progression in breast cancer through induction of ZEB1 expression (41,42), which could in part explain the elevated protein levels of ZEB1 that we observed in the retinoblastoma lines.

The signaling initiated by Nodal and Activin regulates retinal development, supporting retinal progenitor specification from mouse embryonic stem cells (43), and modulating differentiation of WERI Rb1 cells into retinal neurons (22). Activin blocks retinal regeneration from the retinal pigmented epithelium in chicken embryos (44), and inhibits growth in retinoblastoma, inducing differentiation of Y79 cells (45). It is known that Activin often antagonizes the effects of Nodal, and the ligands that activate SMAD2/3 pathway can have opposing effects depending on the cellular type and context (46). Further investigation is warranted to more closely interrogate the functional roles of ACVR1C ligands in regulating retinoblastoma invasion and growth.

MATERIALS AND METHODS

Clinical specimens and RNA-seq analysis

Ten snap frozen retinoblastoma specimens were analyzed by RNA-seq (low input, non-strand specific). Samples were divided in five non-invasive (case 1 to 5: prelaminar, n=4, no optic nerve invasion, n=1) and five invasive (case 6 to 10: retrolaminar, n=4; intralaminar, n=1). Four cases with optic nerve invasion and two without also showed focal (<3mm) choroidal invasion, but none had massive choroidal invasion. Anterior segment invasion was present in two of the invasive cases. The clinical characteristics of the cases are reported in Table S1. These cases were identified through review of pathology and tumor bank records

at King Khaled Eye Specialist Hospital (KKESH), Riyadh, Saudi Arabia. Magnetic Resonance Imaging (MRI) examination was performed to confirm optic nerve invasion (Figure 1a-c). Only tumors with tissue snap-frozen at the time of surgery were used in this study. Two ophthalmic pathologists (Drs. Deepak Edward and Azza Maktabi) reviewed the histopathological slides to confirm the presence of retinoblastoma and the extent of invasion.

Cell cultures, plasmids and chemical reagents

WERI-Rb1 (47) and Y79 (48) human retinoblastoma cells lines were obtained from American Type Culture Collection (ATCC, Manassas, VA). RB143 was obtained from Kerafast, Inc. (49). These lines were cultured in RPMI-1640 supplemented with 50 IU/ml penicillin, 50 μg/ml streptomycin, 1% L-glutamine and 10% heat-inactivated fetal bovine serum (FBS), at 37°C in a humidified 5% CO_2 atmosphere. HSJD-RBT-1, HSJD-RBT-2, patient-derived primary lines which grow in serum-free medium, and HSJD-RBVS-10, a serum-free line derived from tumor seeding in the vitreous, kindly provided by Dr. Carcaboso, were maintained in tumor stem medium, supplemeted with B-27 (Thermo Fisher, Waltham, MA), recombinant EGF, FGF, PDGF-AA/BB (Peprotech, Rocky Hill, NJ) and heparin solution (Sigma-Aldrich, St. Louis, MO), as previously described (50). PANC-1 cells (pancreatic cancer line), kindly provided by Dr. Michael Goggins (Johns Hopkins University), were used as a positive control for SMAD3 phosphorylation, upon treatment for 2 hours with TGF-β1 (Peprotech) at 10 ng/mL. All the cell lines were tested periodically for mycoplasma contamination and STR profiling. pLKO.1 transfer vectors containing short hairpin RNA (shRNA) targeting *ACRV1C, SMAD2,* or *SMAD3* mRNA (sequences are described in Table S2) were purchased from Thermo Fisher. Plasmidic DNA was isolated using PureLink® HiPure Plasmid Midiprep kit (cat. # K210014, Invitrogen, Carlsbad, CA). Lentiviral particles carrying these constructs were prepared using HEK293T as previously described (49). Puromycin (1 μg/mL) was used to select cells expressing the transfer vector. Scrambled shRNAs were used as control. SB505124, a selective inhibitor of ALK4/5/7 receptors (23), was purchased from MedChemExpress, Monmouth Junction, NJ (cat. # HY-13521) and dissolved in DMSO at the stock concentration of 10 mM, following manufacturer's protocol. Recombinant human Nodal ligand was purchased from R&D Systems Inc., Minneapolis, MN (cat. #3218-ND-025).

RNA extraction and quantitative real-time PCR

RNeasy mini kit (Qiagen, Germantown, MD) was used to perform RNA extraction from retinoblastoma cell lines, with on-column DNA digestion carried out with RNase-free DNase kit (Qiagen), to eliminate genomic DNA. Quantitative real-time PCR (qPCR) for ACVR1C/SMAD2 pathway components was carried out as previously described (51), with primer sequences listed in Table S3. Each experiment was performed three times and all reactions were carried out in triplicates in iQ5 Multicolor real-time PCR detection system (Bio-Rad, Hercules, CA), using SYBR Green (Applied Biosystems, Foster City, CA) as fluorescent dye; β-actin mRNA levels were used to normalize the results.

RNA-seq analysis

Ten snap frozen retinoblastoma specimens were analyzed by RNA-seq (low input, non-strand specific). For our low input RNA library preparation workflow, the quality of total

RNA was measured by the Agilent Bioanalyzer (Santa Clara, CA) utilizing a RNA Pico chip to generate a RIN score. High quality RNA (>7.0 RIN) was used to generate a library for sequencing. Starting with 500 pg - 100 ng of total RNA, generation of cDNA was prepared as directed in the Nugen Ovation RNA-Seq System V2 Sample Preparation Guide. After purification of the cDNA was complete, construction of the sequencing library was prepared as directed in the Illumina TruSeq DNA sample preparation guide. Fragmentation was performed on the Covaris S2. PCR was performed to selectively enrich DNA fragments which have adaptor molecules and to amplify the amount of the library itself. Libraries were run on a High Sensitivity chip using the Agilent Bioanalyzer to assess size distribution and overall quality of the amplified library. Quantification of the libraries was performed by qPCR with the Kappa Library Quantification Kit or by the Agilent Bioanalyzer and equimolar concentrations of each library were pooled together. Cluster generation and sequencing was performed on an Illumina HS2500 platform for a 100bp x 100bp, paired end sequencing utilizing the TruSeq Rapid PE Cluster Kit and TruSeq Rapid SBS Kit (200 cycles) respectively. Data analysis was performed using Integrative Genomics Viewer (IGV) software (52). All RNA-seq data generated during this study are included in this article (and its supplementary information files).

Western blotting

The protein levels of total and phospho-SMAD2/3, ZEB1, Snail, and cleaved poly (ADP-ribose) polymerase (PARP) were evaluated by Western blot in retinoblastoma cells, with β-Actin used as a loading control. Proteins were extracted using TNE lysis buffer, as previously described (49). 4–12% SDS–polyacrylamide gel electrophoresis (Invitrogen), was used to separate equal amounts of proteins, which were then transferred on a nitrocellulose membrane (Invitrogen) and incubated for 1 hour in blocking solution containing 5% dried milk in TBS with 0.1% Tween 20 (TBS-T). Membranes were incubated with the primary antibodies overnight in blocking solution at 4°C. The following primary antibodies were used: total and phospho-SMAD2/3 (in rabbit, 1:1000, Cell Signaling Technology, SMAD2/3 sampler kit #12747, Danvers, MA), ZEB1 (in rabbit, 1:2000, Sigma-Aldrich, # HPA027524, St. Louis, MO), Snail (in mouse, 1:1000, Cell Signaling Technology, #3895, Danvers, MA), cleaved poly (ADP-ribose) polymerase (PARP), cleaved PARP at Asp^{214} (in rabbit, 1:1000, Cell Signaling Technology, #5625), Nodal (in mouse, 1:800, Sigma-Aldrich, #SAB1404135), GDF3 (in mouse, 1:500, Sigma-Aldrich, #SAB1406848), β-Actin (in mouse, 1:500, Santa Cruz Biotechnology, # sc-47778, Dallas, TX). Secondary antibodies bound to peroxidase and raised in mouse or in rabbit (1:3000, Cell Signaling Technology, #7074, #7076) were used to visualize protein bands. Enhanced chemiluminescence (ECL) was used as detection reagent (PerkinElmer, Waltham, MA).

Cell growth, proliferation, apoptosis and transwell invasion assays

Cell growth assay.—Cell Counting-Kit 8 (CCK-8, Sigma-Aldrich), containing WST-8 reagent [2-(2-methoxy-4-nitrophenyl)-3-(4-nitrophenyl)-5-(2,4-disulfophenyl)-2H-tetrazolium, monosodium salt], was utilized to measure growth, as previously described (51). Each experimental condition has been repeated in biological triplicate and data are presented as mean ± standard deviation (SD).

Proliferation assay.—Cell replication was measured by Ki67 immunoassay, using Muse® Cell Analyzer (Millipore, Billerica, MA), following manufacturer's instructions for cells in non-adherent conditions.

Apoptosis assay.—Activation of the apoptotic pathway in retinoblastoma cells treated with SB505124 was determined by immunofluorescence, using cleaved caspase-3 antibody (in rabbit, 1:400, Cell Signaling Technology, #9661), as previously described (53).

Invasion assay.—Cellular invasion was determined by transwell invasion assay, as previously described (49). After incubation for 72 hours, cells that had migrated through the Matrigel-coated filter floated in the medium located in the lower chamber. The amount of viable floating cells was determined in this chamber by trypan blue exclusion dye. Only the unstained/viable cells were counted, excluding the possibility that reduction in cell invasion could be attributable to apoptosis. Data indicate the mean (± SD) of each of three independent experiments (biological triplicate).

Immunofluorescence assay

Nodal expression was determined in WERI Rb1 and Y79 cells by immunofluorescence, using anti-Nodal antibody (in mouse, 1:100, Sigma-Aldrich, #SAB1404135), following the same protocol as for the cleaved caspase-3 assay (51). PANC-1 cells were used as positive control, while incubation without primary antibody in all three lines was used as negative control. Incubation with secondary antibody was carried out with cyanine Cy™-3 conjugated AffiniPure anti-mouse IgG (1:500, Jackson ImmunoResearch Laboratories Inc., West Grove, PA).

Zebrafish tumor cell xenotransplantation

The zebrafish background strain was "AB", from the Zebrafish International Resource Center (ZIRC). Zebrafish were maintained using established temperature and light cycle conditions (28.5°C, 14 hours of light/10 hours of dark). All experimental procedures were approved by the Animal Care and Use Committee of Johns Hopkins University. For zebrafish xenotransplantation, we followed a prior procedure (54), modified specifically for modeling retinoblastoma (55). At 2 days post fertilization (dpf), $roy^{a9/a9}$ strains of zebrafish embryos were dechorionated and anaesthetized in 1.0× Embryo Medium (E3) containing phenythiourea (PTU, Sigma-Aldrich) and 0.04 mg/ml tricaine (Sigma-Aldrich), before human retinoblastoma cell injection. Approximately 60–80 Y79 cells, labelled with GFP-MSCV retroviral vector (56), were injected (Dagan PMI-100 microinjector) into the vitreous cavity of each embryo. Afterwards larvae were transferred to an incubator and maintained at 28.5°C overnight. At 1 day post-injection (dpi) larvae were screened for visible GFP^+ cell mass at injection site via stereo fluorescence microscopy (Olympus SZX16, Center Valley, PA). The localization of the GFP expressing retinoblastoma cells was monitored by confocal intravital microscopy (Olympus FV1000) at 1 and 4 dpi, to determine whether pharmacological or genetic manipulation of the Nodal/TGF-β pathway altered the metastatic spread of the retinoblastoma cells outside the eye. The extent of retinoblastoma metastasis was determined using IMARIS & Matlab software, as previously described (57,58). Zebrafish studies used at least 11 animals per group in order to give 80% power to detect a

difference between means of over 20% with a significance level of 0.05 (two-tailed). No randomization or blinding were used for the animal studies. We could not account for male/female selection in the fish experiments, as they do not undergo sexual selection until about 4 weeks of development, and we use zebrafish larvae up to 8 days post-fertilization.

Statistical Analysis

Experiments were performed in biological triplicate and data are presented as the mean ± standard deviation (SD). Levels of significance were determined by two-sided Student *t*-test or by one-way ANOVA, with p values lower than 0.05 considered statistically significant. Statistical calculations were performed using GraphPad Prism5 software (San Diego, CA). Regarding the *in vivo* analyses, data were processed with a custom R-based package (ggplot2, 59) to generate box plots showing the first quartile (lower box), median (bold line), third quartile (upper box), upper and lower adjacent (whiskers), and raw data (dot plot; large dots denote outlier observations) for each experimental condition. Statistical analyses were carried out with R 3.3.1 and RStudio 0.99.893. Student's *t* test was used to calculate effect size between paired groups, with effect size, 95% confidence intervals (CI), and *P* values provided.

Supplementary Material

Refer to Web version on PubMed Central for supplementary material.

ACKNOWLEDGEMENTS

We thank Jennifer Meyers for her technical assistance in the RNA-seq, Dr. Wayne Yu for pathway analysis, Dr. Michael Goggins for providing PANC-1 cells, and Urvi Patel for technical support. RNA-seq analysis was conducted at The Sidney Kimmel Cancer Center, Next Generation Sequencing Core at the Johns Hopkins University. This study was supported by King Khaled Eye Specialist Hospital (KKESH) – Wilmer Eye Institute (WEI) Collaborative Research Grant, by the NIH Grant R21CA229919, the core grant EY001765 and by The Jenny Fund. AMC acknowledges funding from ISCIII-FEDER (CP13/00189) and MINECO (Retos program; Cure4RB project RTC-2015–4319-1).

Financial support: King Khaled Eye Specialist Hospital (KKESH) – Wilmer Eye Institute (WEI) Collaborative Research Grant, NIH Grant R21CA229919, the core grant EY001765, and The Jenny Fund. AMC acknowledges funding from ISCIII-FEDER (CP13/00189) and MINECO (Retos program; Cure4RB project RTC-2015–4319-1).

REFERENCES

1. Honavar SG, Singh AD. Management of advanced retinoblastoma. Ophthalmol Clin North Am 2005; 18: 65–73. [PubMed: 15763192]
2. Chantada GL, Qaddoumi I, Canturk S, Khetan V, Ma Z, Kimani K, et al. Strategies to manage retinoblastoma in developing countries. Pediatr Blood Cancer 2011; 56: 341–348. [PubMed: 21225909]
3. Villegas VM, Hess DJ, Wildner A, Gold AS, Murray TG. Retinoblastoma. Curr Opin Ophthalmol 2013; 24: 581–588. [PubMed: 24100372]
4. Bondestam J, Huotari MA, Morén A, Ustinov J, Kaivo-Oja N, Kallio J, et al. cDNA cloning, expression studies and chromosome mapping of human type I serine/threonine kinase receptor ALK7 (ACVR1C). Cytogenet Cell Genet 2001; 95: 157–62. [PubMed: 12063393]
5. Shi Y, Massagué J. Mechanisms of TGF-beta signaling from cell membrane to the nucleus.Cell 2003; 113: 685–700. [PubMed: 12809600]
6. Loomans HA, Andl CD. Activin receptor-like kinases: a diverse family playing an important role in cancer. Am J Cancer Res 2016; 6: 2431–2447. [PubMed: 27904762]

7. Tsuchida K, Nakatani M, Hitachi K, Uezumi A, Sunada Y, Ageta H, et al. Activin signaling as an emerging target for therapeutic interventions. Cell Commun Signal 2009; 7: 15. [PubMed: 19538713]
8. Peng L, Yuan XQ, Zhang CY, Ye F, Zhou HF, Li WL, et al. High TGF-β1 expression predicts poor disease prognosis in hepatocellular carcinoma patients. Oncotarget 2017; 8: 34387–34397. [PubMed: 28415739]
9. Lonardo E, Hermann PC, Mueller MT, Huber S, Balic A, Miranda-Lorenzo I, et al. Nodal/Activin signaling drives self-renewal and tumorigenicity of pancreatic cancer stem cells and provides a target for combined drug therapy. Cell Stem Cell 2011; 9: 433–446. [PubMed: 22056140]
10. Lawrence MG, Margaryan NV, Loessner D, Collins A, Kerr KM, Turner M, et al. Reactivation of embryonic nodal signaling is associated with tumor progression and promotes the growth of prostate cancer cells. Prostate 2011; 71: 1198–1209. [PubMed: 21656830]
11. Kirsammer G, Strizzi L, Margaryan NV, Gilgur A, Hyser M, Atkinson J, et al. Nodal signaling promotes a tumorigenic phenotype in human breast cancer. Semin Cancer Biol 2014; 29: 40–50. [PubMed: 25073112]
12. Bashir M, Damineni S, Mukherjee G, Kondaiah P. Activin-A signaling promotes epithelial–mesenchymal transition, invasion, and metastatic growth of breast cancer. NPJ Breast Cancer 2015; 1: 15007. [PubMed: 28721365]
13. Condro MC, Matynia A, Foster NN, Ago Y, Rajbhandari AK, Van C, et al. High-resolutioncharacterization of a PACAP-EGFP transgenic mouse model for mapping PACAP-expressing neurons. J Comp Neurol 2016; 524: 3827–3848. [PubMed: 27197019]
14. Morini M, Astigiano S, Gitton Y, Emionite L, Mirisola V, Levi G, et al. Mutually exclusive expression of DLX2 and DLX5/6 is associated with the metastatic potential of the human breast cancer cell line MDA-MB-231. BMC Cancer 2010; 10: 649. [PubMed: 21108812]
15. Chung IC, Chen LC, Chung AK, Chao M, Huang HY, Hsueh C, et al. Matrix metalloproteinase 12 is induced by heterogeneous nuclear ribonucleoprotein K and promotes migration and invasion in nasopharyngeal carcinoma. BMC Cancer 2014; 14: 348. [PubMed: 24885469]
16. Lv FZ, Wang JL, Wu Y, Chen HF, Shen XY. Knockdown of MMP12 inhibits the growth and invasion of lung adenocarcinoma cells. Int J Immunopathol Pharmacol 2015; 28: 77–84. [PubMed: 25816409]
17. White CD, Brown MD, Sacks DB. IQGAPs in cancer: a family of scaffold proteins underlying tumorigenesis. FEBS Lett 2009; 583: 1817–24. [PubMed: 19433088]
18. Yang Y, Zhao W, Xu QW, Wang XS, Zhang Y, Zhang J. IQGAP3 promotes EGFR-ERK signaling and the growth and metastasis of lung cancer cells. PLoS One 2014; 9:e97578. [PubMed: 24849319]
19. Schubert FR, Sobreira DR, Janousek RG, Alvares LE, Dietrich S. Dact genes are chordate specific regulators at the intersection of Wnt and Tgf-β signaling pathways. BMC Evol Biol 2014; 14: 157. [PubMed: 25099342]
20. Postovit LM, Margaryan NV, Seftor EA, Kirschmann DA, Lipavsky A, Wheaton WW, et al. Human embryonic stem cell microenvironment suppresses the tumorigenic phenotype of aggressive cancer cells. *Proc Natl Acad Sci* USA 2008; 105: 4329–4334. [PubMed: 18334633]
21. Tanaka K, Imoto I, Inoue J, Kozaki K, Tsuda H, Shimada Y, et al. Frequent methylation-associated silencing of a candidate tumor-suppressor, CRABP1, in esophageal squamous-cell carcinoma. Oncogene 2007; 26: 6456–6468. [PubMed: 17438526]
22. Liu Y, Hu H, Liang M, Xiong Y, Li K, Chen M, et al. Regulated differentiation of WERI-Rb-1 cells into retinal neuron-like cells. Int J Mol Med 2017; 40: 1172–1184. [PubMed: 28848998]
23. DaCosta Byfield S, Major C, Laping NJ, Roberts AB. SB-505124 is a selective inhibitor of transforming growth factor-beta type I receptors ALK4, ALK5, and ALK7. Mol Pharmacol 2004; 65: 744–752. [PubMed: 14978253]
24. Leal-Leal CA, Rivera-Luna R, Flores-Rojo M, Juárez-Echenique JC, Ordaz JC, Amador-Zarco J. Survival in extra-orbital metastatic retinoblastoma:treatment results. Clin Transl Oncol 2006; 8: 39–44. [PubMed: 16632438]
25. Busch M, Papior D, Stephan H, Dünker N. Characterization of etoposide- and cisplatin-chemoresistant retinoblastoma cell lines. Oncol Rep 2018; 39: 160–172. [PubMed: 29192327]

26. Badhu B, Sah SP, Thakur SK, Dulal S, Kumar S, Sood A, et al. Clinical presentation of retinoblastoma in Eastern Nepal. Clin Experiment Ophthalmol 2005; 33: 386–389. [PubMed: 16033351]
27. Chawla B, Hasan F, Seth R, Pathy S, Pattebahadur R, Sharma S, et al. Multimodal Therapy for Stage III Retinoblastoma (International Retinoblastoma Staging System): A Prospective Comparative Study. Ophthalmology 2016; 123: 1933–1939. [PubMed: 27449712]
28. James D, Levine AJ, Besser D, Hemmati-Brivanlou A. TGFbeta/activin/nodal signaling is necessary for the maintenance of pluripotency in human embryonic stem cells. Development 2005; 132: 1273–1282. [PubMed: 15703277]
29. Massagué J TGFbeta in Cancer. Cell 2008; 134: 215–230. [PubMed: 18662538]
30. Topczewska JM, Postovit LM, Margaryan NV, Sam A, Hess AR, Wheaton WW, et al. Embryonic and tumorigenic pathways converge via Nodal signaling: role in melanoma aggressiveness. Nat Med 2006; 12: 925–32. [PubMed: 16892036]
31. Strizzi L, Postovit LM, Margaryan NV, Lipavsky A, Gadiot J, Blank C, et al. Nodal as a biomarker for melanoma progression and a new therapeutic target for clinical intervention. Expert Rev Dermatol 2009; 4: 67–78. [PubMed: 19885369]
32. Hu T, Su F, Jiang W, Dart DA. Overexpression of Activin Receptor-like Kinase 7 in Breast Cancer Cells Is Associated with Decreased Cell Growth and Adhesion. Anticancer Res 2017; 37: 3441–3451. [PubMed: 28668833]
33. Pacifici M, Shore EM. Common mutations in ALK2/ACVR1, a multi-faceted receptor, have roles in distinct pediatric musculoskeletal and neural orphan disorders. Cytokine Growth Factor Rev 2016; 27: 93–104. [PubMed: 26776312]
34. Gong W, Sun B, Zhao X, Zhang D, Sun J, Liu T, et al. Nodal signaling promotes vasculogenic mimicry formation in breast cancer via the Smad2/3 pathway. Oncotarget 2016; 7: 70152–70167. [PubMed: 27659524]
35. Yoshinaga K, Inoue H, Utsunomiya T, Sonoda H, Masuda T, Mimori K, et al. N-cadherin is regulated by activin A and associated with tumor aggressiveness in esophageal carcinoma. Clin Cancer Res 2004; 10: 5702–5707. [PubMed: 15355896]
36. Schmierer B, Schuster MK, Shkumatava A, Kuchler K. Activin A signaling induces Smad2, but not Smad3, requiring protein kinase A activity in granulosa cells from the avian ovary. J Biol Chem. 2003; 278: 21197–203. [PubMed: 12665510]
37. Liu C, Gaça MD, Swenson ES, Vellucci VF, Reiss M, Wells RG. Smads 2 and 3 are differentially activated by transforming growth factor-beta (TGF-beta) in quiescent and activated hepatic stellate cells. Constitutive nuclear localization of Smads in activated cells is TGF-beta-independent. J Biol Chem. 2003; 278: 11721–8. [PubMed: 12547835]
38. Kalluri R, Weinberg RA. The basics of epithelial–mesenchymal transition. J Clin Investig 2009; 119: 1420–1428. [PubMed: 19487818]
39. Gregory PA, Bracken CP, Smith E, Bert AG, Wright JA, Roslan S, et al. An autocrine TGF-β/ZEB/miR-200 signaling network regulates establishment and maintenance of epithelial-mesenchymal transition. Mol Biol Cell 2011; 22: 1686–1698. [PubMed: 21411626]
40. Joseph JV, Conroy S, Tomar T, Eggens-Meijer E, Bhat K, Copray S, et al. TGF-β is an inducer of ZEB1-dependent mesenchymal transdifferentiation in glioblastoma that is associated with tumor invasion. Cell Death Dis 2014; 5:e1443. [PubMed: 25275602]
41. Arima Y, Hayashi H, Sasaki M, Hosonaga M, Goto TM, Chiyoda T, et al. Induction of ZEB proteins by inactivation of RB protein is key determinant of mesenchymal phenotype of breast cancer. J Biol Chem 2012; 287: 7896–7906. [PubMed: 22262832]
42. Liu Y, Sánchez-Tilló E, Lu X, Huang L, Clem B, Telang S, et al. Sequential inductions of the ZEB1 transcription factor caused by mutation of Rb and then Ras proteins are required for tumor initiation and progression. J Biol Chem 2013; 288: 11572–11580. [PubMed: 23443660]
43. Bertacchi M, Lupo G, Pandolfini L, Casarosa S, D'Onofrio M, Pedersen RA, et al. Activin/Nodal Signaling Supports Retinal Progenitor Specification in a Narrow Time Window during Pluripotent Stem Cell Neuralization. Stem Cell Reports 2015; 5: 532–545. [PubMed: 26388287]
44. Sakami S, Etter P, Reh TA. Activin signaling limits the competence for retinal regeneration from the pigmented epithelium. Mech Dev 2008; 125: 106–16. [PubMed: 18042353]

45. Kanno C, Kashiwagi Y, Horie K, Inomata M, Yamamoto T, Kitanaka C, et al. Activin inhibits cell growth and induces differentiation in human retinoblastoma Y79 cells. Curr Eye Res 2009; 34: 652–659. [PubMed: 19899992]
46. Gray PC, Vale W. Cripto/GRP78 modulation of the TGF-β pathway in development and oncogenesis. FEBS Lett 2012; 586: 1836–1845. [PubMed: 22306319]
47. McFall RC, Sery TW, Makadon M. Characterization of a new continuous cell line derived from a human retinoblastoma. Cancer Res 1977; 37: 1003–1010. [PubMed: 844036]
48. Reid TW, Albert DM, Rabson AS, Russell P, Craft J, Chu EW, et al. Characteristics of an established cell line of retinoblastoma. J Natl Cancer Inst 1974; 53: 347–360. [PubMed: 4135597]
49. Theodoropoulou S, Kolovou PE, Morizane Y, Kayama M, Nicolaou F, Miller JW et al. Retinoblastoma cells are inhibited by aminoimidazole carboxamide ribonucleotide (AICAR) partially through activation of AMP-dependent kinase. FASEB J 2010; 24: 2620–30. [PubMed: 20371623]
50. Pascual-Pasto G, Olaciregui NG, Vila-Ubach M, Paco S, Monterrubio C, Rodriguez E, et al.Preclinical platform of retinoblastoma xenografts recapitulating human disease and molecular markers of dissemination. Cancer Lett 2016; 380: 10–19. [PubMed: 27319373]
51. Asnaghi L, Tripathy A, Yang Q, Kaur H, Hanaford A, Yu W, et al. Targeting Notch signaling as a novel therapy for Retinoblastoma. Oncotarget 2016; 7: 70028–70044. [PubMed: 27661116]
52. Robinson JT, Thorvaldsdóttir H, Winckler W, Guttman M, Lander ES, Getz G, et al. Integrative genomics viewer. Nat Biotechnol 2011; 29: 24–26. [PubMed: 21221095]
53. Weingart MF, Roth JJ, Hutt-Cabezas M, Busse TM, Kaur H, Price A, et al. Disrupting LIN28 in atypical teratoid rhabdoid tumors reveals the importance of the mitogen activated protein kinase pathway as a therapeutic target. Oncotarget 2015; 6: 3165–3177. [PubMed: 25638158]
54. Teng Y, Xie X, Walker S, White DT, Mumm JS, Cowell JK. Evaluating human cancer cell metastasis in zebrafish. BMC Cancer 2013; 13: 453. [PubMed: 24089705]
55. Chen X, Wang J, Cao Z, Hosaka K, Jensen L, Yang H, et al. Invasiveness and metastasis of retinoblastoma in an orthotopic zebrafish tumor model. Sci Rep 2015; 5:10351. [PubMed: 26169357]
56. Asnaghi L, Handa JT, Merbs SL, Harbour JW, Eberhart CG. A role for Jag2 in promoting uveal melanoma dissemination and growth. Invest Ophthalmol Vis Sci 2013; 54: 295–306. [PubMed: 23211831]
57. Hamilton L, Astell KR, Velikova G, Sieger D. A Zebrafish Live Imaging Model Reveals Differential Responses of Microglia Toward Glioblastoma Cells In Vivo. Zebrafish 2016; 13: 523–534. [PubMed: 27779463]
58. White DT, Sengupta S, Saxena MT, Xu Q, Hanes J, Ding D, et al. Immunomodulation-Accelerated neuronal regeneration following selective rod photoreceptor cell ablation in the zebrafish retina. *Proc Natl Acad Sci* USA 2017; 14: E3719–E3728.
59. Wickham H ggplot2 - Elegant Graphics for Data Analysis. 2nd Ed Springer International Publishing, Cham, Switzerland, 2016.

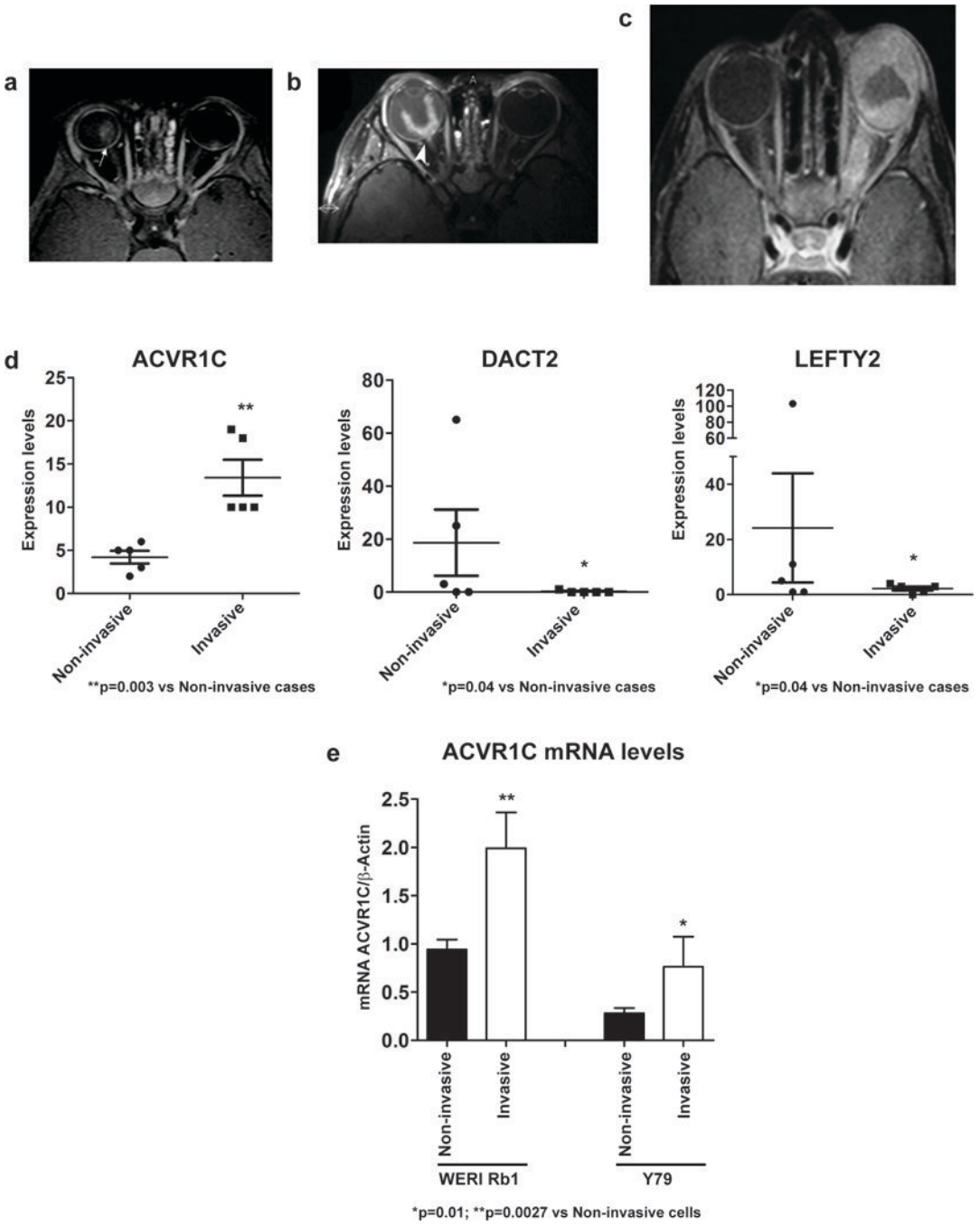

Figure 1. ACVR1C mRNA levels were significantly increased in invasive retinoblastoma cells.

a-c: Representative images of the MRI evaluation of the optic nerve invasion in the retinoblastoma cases. **a**: Axial T1 WI post contrast fat suppression of case #2 shows bilateral retinoblastoma with clear delineation of a continuous choroidal-retinal line with no sign of optic nerve invasion (arrow). **b**: Axial T1-weighted post contrast, fat-suppressed image of case #8: retinoblastoma with post laminar optic nerve invasion (arrowhead). **c**: Axial post contrast T1WI, fat-suppressed image of case #9: retinoblastoma which diffusely infiltrated the sclera and the optic nerve. **d**: The mRNA levels of ACVR1C were significantly increased

in all five invasive cases, while those of DACT2 and LEFTY2 were significantly decreased in most of the invasive cases. Expression levels were obtained from the RNA-seq analysis. Probability of differential expression: PPDE=0.814 (ACVR1C); PPDE=0.995 (DACT2); PPDE=0.892 (LEFTY2). **e**: ACVR1C mRNA levels were significantly increased in invasive WERI Rb1 and Y79 cells, as compared to non-invasive cells. Transwell invasion assay was used to separate the invasive cells, present in the lower side of a Matrigel-coated filter, from the non-invasive, present inside of the insert, after 72 hours of incubation, following a previous procedure (54).

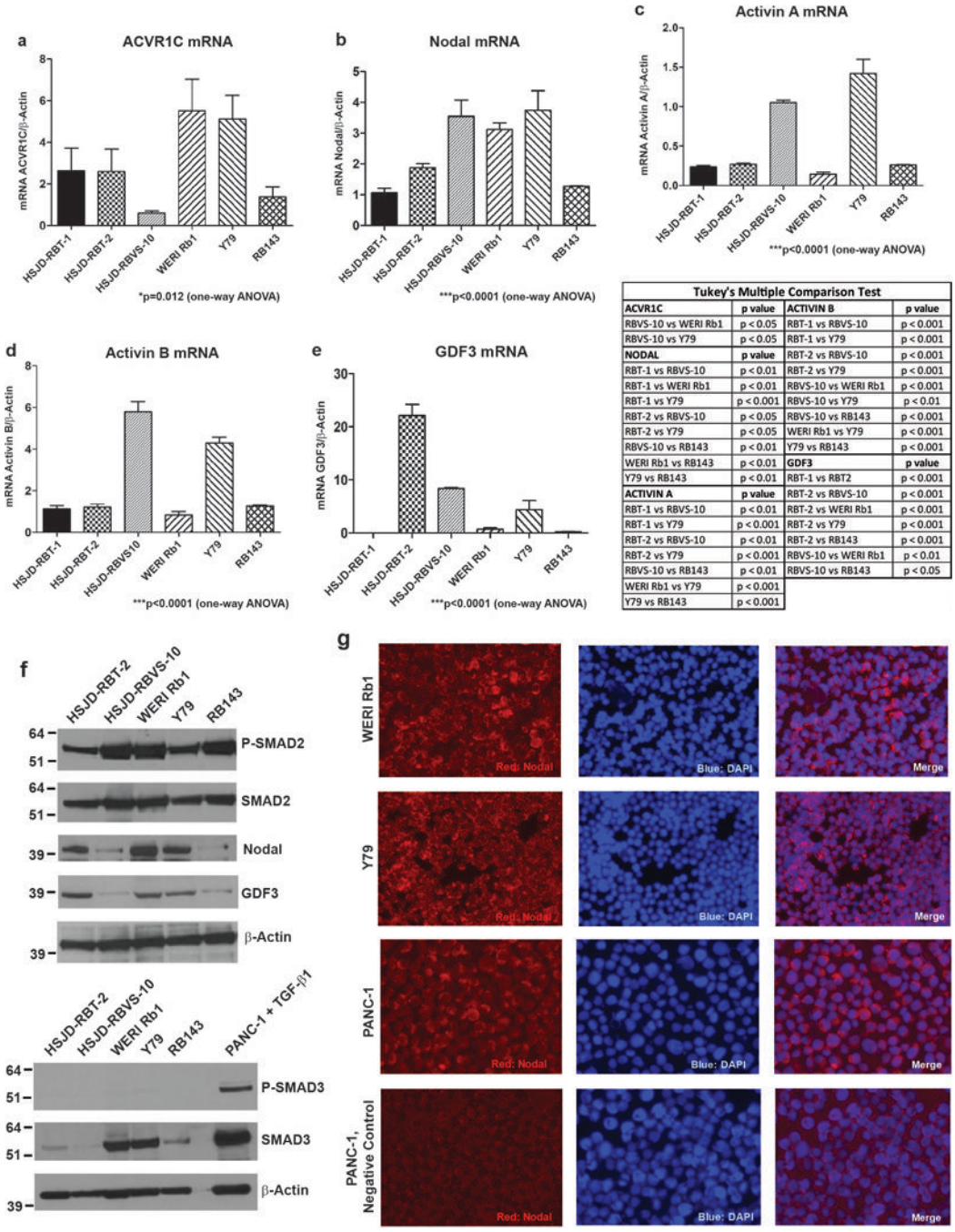

Tukey's Multiple Comparison Test			
ACVR1C	**p value**	**ACTIVIN B**	**p value**
RBVS-10 vs WERI Rb1	p < 0.05	RBT-1 vs RBVS-10	p < 0.001
RBVS-10 vs Y79	p < 0.05	RBT-1 vs Y79	p < 0.001
NODAL	**p value**	RBT-2 vs RBVS-10	p < 0.001
RBT-1 vs RBVS-10	p < 0.01	RBT-2 vs Y79	p < 0.001
RBT-1 vs WERI Rb1	p < 0.01	RBVS-10 vs WERI Rb1	p < 0.001
RBT-1 vs Y79	p < 0.001	RBVS-10 vs Y79	p < 0.01
RBT-2 vs RBVS-10	p < 0.05	RBVS-10 vs RB143	p < 0.001
RBT-2 vs Y79	p < 0.05	WERI Rb1 vs Y79	p < 0.001
RBVS-10 vs RB143	p < 0.01	Y79 vs RB143	p < 0.001
WERI Rb1 vs RB143	p < 0.01	**GDF3**	**p value**
Y79 vs RB143	p < 0.01	RBT-1 vs RBT2	p < 0.001
ACTIVIN A	**p value**	RBT-2 vs RBVS-10	p < 0.001
RBT-1 vs RBVS-10	p < 0.01	RBT-2 vs WERI Rb1	p < 0.001
RBT-1 vs Y79	p < 0.001	RBT-2 vs Y79	p < 0.001
RBT-2 vs RBVS-10	p < 0.01	RBT-2 vs RB143	p < 0.001
RBT-2 vs Y79	p < 0.001	RBVS-10 vs WERI Rb1	p < 0.01
RBVS-10 vs RB143	p < 0.01	RBVS-10 vs RB143	p < 0.05
WERI Rb1 vs Y79	p < 0.001		
Y79 vs RB143	p < 0.001		

Figure 2. Expression of ACVR1C/SMAD2 pathway components in retinoblastoma lines.

The mRNA levels of ACVR1C receptor (**a**) and ligands (**b-e**) in multiple retinoblastoma lines were determined by qPCR. P values were calculated using one-way analysis of the variance (ANOVA), with post-hoc Tukey's test in the table. Levels of phospho- and total SMAD2/3 proteins, Nodal and GDF3 ligands in retinoblastoma lines were evaluated by Western blot (**f**), using β-Actin as loading control. Pancreatic cancer cell line PANC-1, treated with TGF-β1 at 10 ng/mL for 2 hours, was used as positive control for phospho-SMAD3 antibody. Nodal expression was determined in WERI Rb1 and Y79 cells by

immunofluorescence (**g**), using anti-Nodal antibody (red). Nuclei were stained with DAPI (blue). PANC-1 cells were used as positive control.

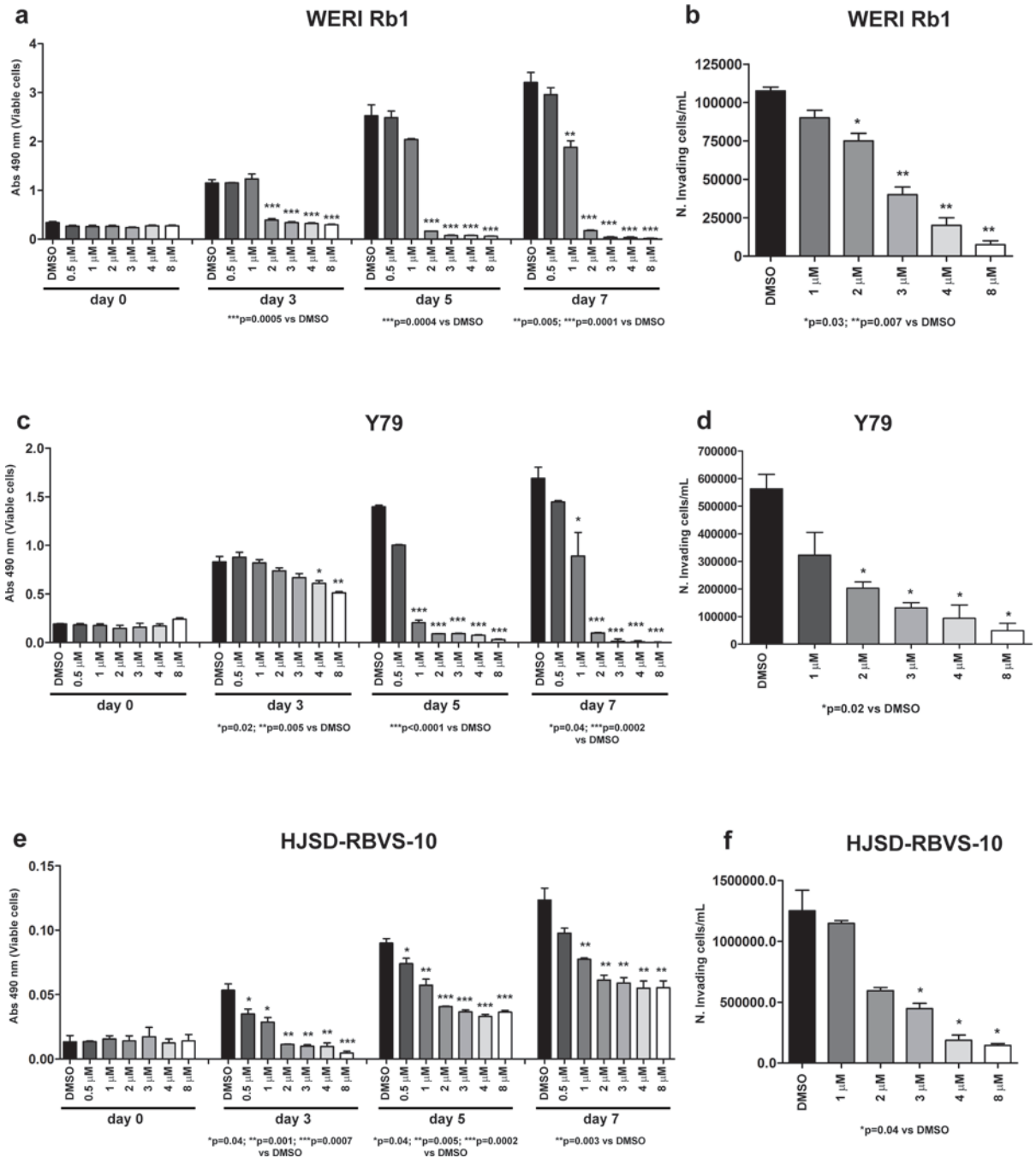

Figure 3. Pharmacological inhibition of the ACVR1C/SMAD2 pathway using SB505124 represses growth and invasion in retinoblastoma cells.

a, c, e: Growth was inhibited in a dose-dependent manner in WERI Rb1 (**a**), Y79 (**c**), and HSJD-RBVS-10 (**e**) cells treated with SB505124 for 3, 5, 7 days at the indicated doses, as found by CCK-8 assay. P values were calculated using two-sided Student *t*-test vs DMSO-treated cells. Data are presented as the mean ± SD. **b, d, f:** The ability of the cells to invade a Matrigel-coated filter was reduced in a dose-dependent manner in WERI Rb1 (**b**), Y79 (**d**),

and HSJD-RBVS-10 (**f**) cells treated with SB505124 for 3 days at the indicated doses, as found by transwell invasion assay.

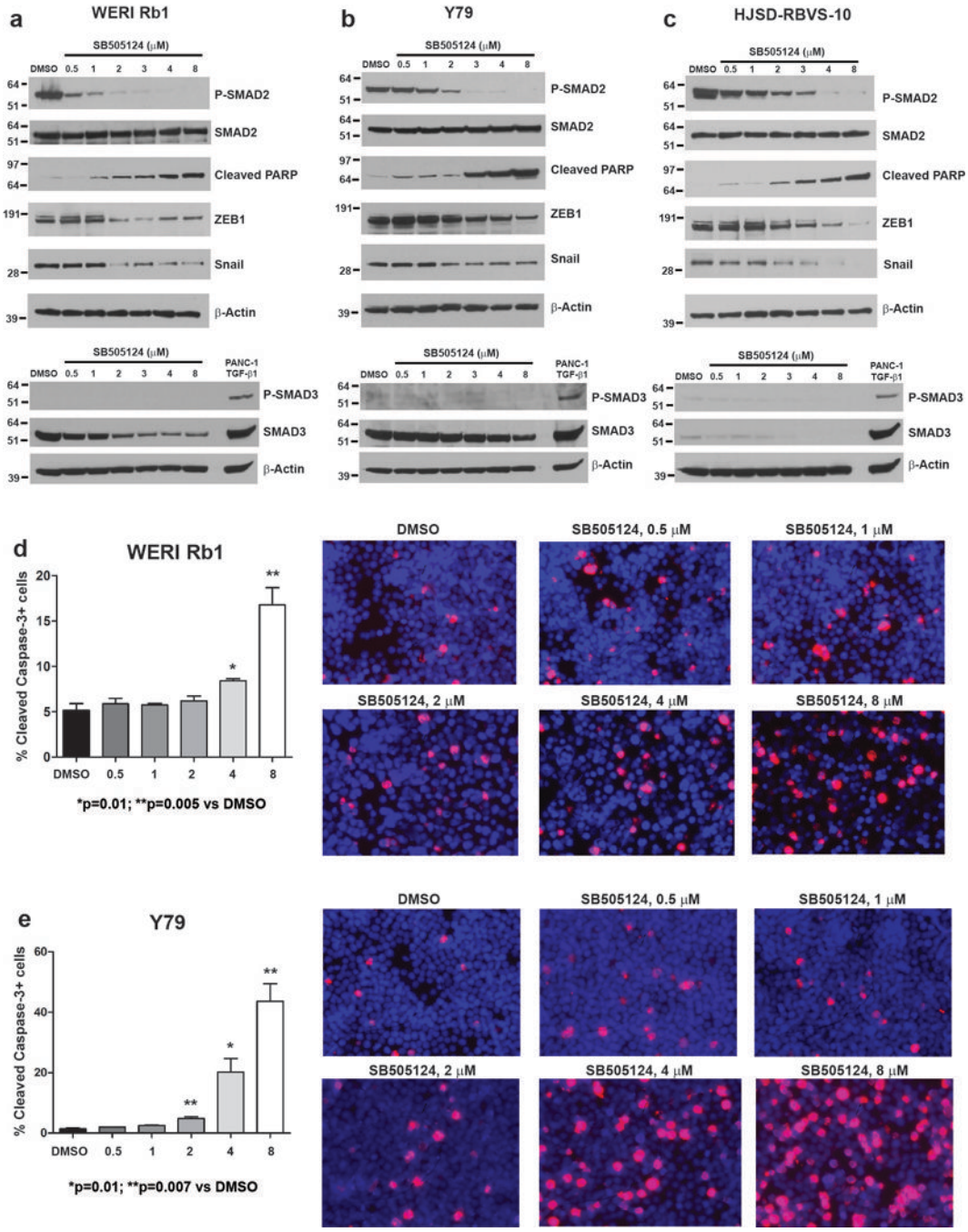

Figure 4. Pharmacological inhibition of the ACVR1C/SMAD2 pathway induces apoptosis and inhibits the expression of EMT markers in retinoblastoma cells.

a-c: Phosphorylation of SMAD2 was reduced in a dose-dependent manner in WERI Rb1 (**a**), Y79 (**b**), HSJD-RBVS-10 (**c**) cells treated with SB505124 for 4 days at the indicated doses, as found by Western blot. Induction of cleaved PARP, indicative of apoptosis, and reduction in Snail and ZEB1 protein levels were also observed, starting at the dose of 2 μM. No phosphorylation of SMAD3 was detected in these lines, while a dose-dependent decrease in the protein levels of SMAD3 was observed in WERI Rb1 and Y79 (Figure 4a-b, bottom

panel). PANC-1 cells treated with TGF-β1 at 10 ng/mL for 2 hours were used as positive control for phospho-SMAD3 antibody. **d,e**: Treatment with SB505124 for 3 days significantly increased apoptosis at 4 and 8 μM in WERI Rb1 (**d**) and at 2, 4, 8 μM in Y79 (**e**), compared to DMSO, as determined by immunofluorescence assay using an antibody specific for cleaved caspase-3 (red). P values were calculated using two-sided Student *t*-test vs DMSO-treated cells. Data are presented as mean ± SD. Microphotographs in the right part of the panels are representative images of the immunofluorescence staining. Nuclei were stained with DAPI (blue).

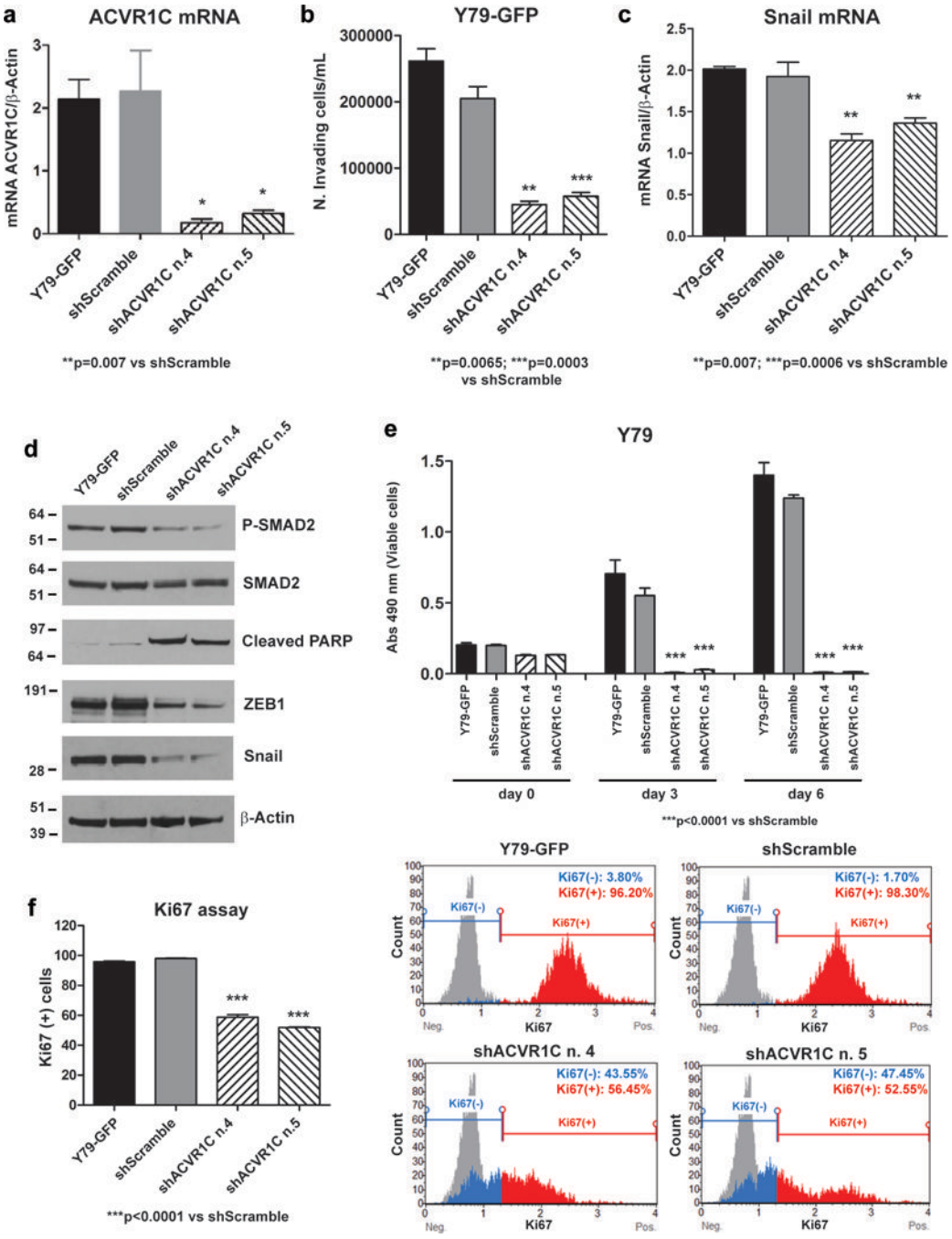

Figure 5. Genetic downregulation of ACVR1C inhibits invasion, growth and proliferation in Y79 cells.

ACVR1C (**a**) and Snail (**c**) mRNA levels were determined by qPCR in Y79-GFP cells transduced with ACVR1C shRNAs or scrambled shRNA, and in parental cells. Invasion was reduced by about 70% in Y79-GFP cells expressing ACVR1C shRNAs compared to scrambled shRNA, as determined by transwell invasion assay (**b**). P values were calculated using two-sided Student *t*-test vs scrambled shRNA. Data are presented as mean ± SD. Phosphorylation of SMAD2 and protein levels of Snail and ZEB1 were dramatically reduced

in cells expressing ACVR1C shRNAs as compared to scrambled shRNA, while the apoptotic marker cleaved PARP was increased, as found by Western blot (**d**). Growth was reduced by more than 90% in Y79 cells expressing two different ACVR1C shRNAs, compared to scrambled shRNA, as found by CCK-8 growth assay (**e**). The percentage of Ki67-positive cells was reduced from 40 to 50% in cells transduced with two different ACVR1C shRNAs, compared to scrambled shRNA, as found by Ki67 proliferation assay (**f**).

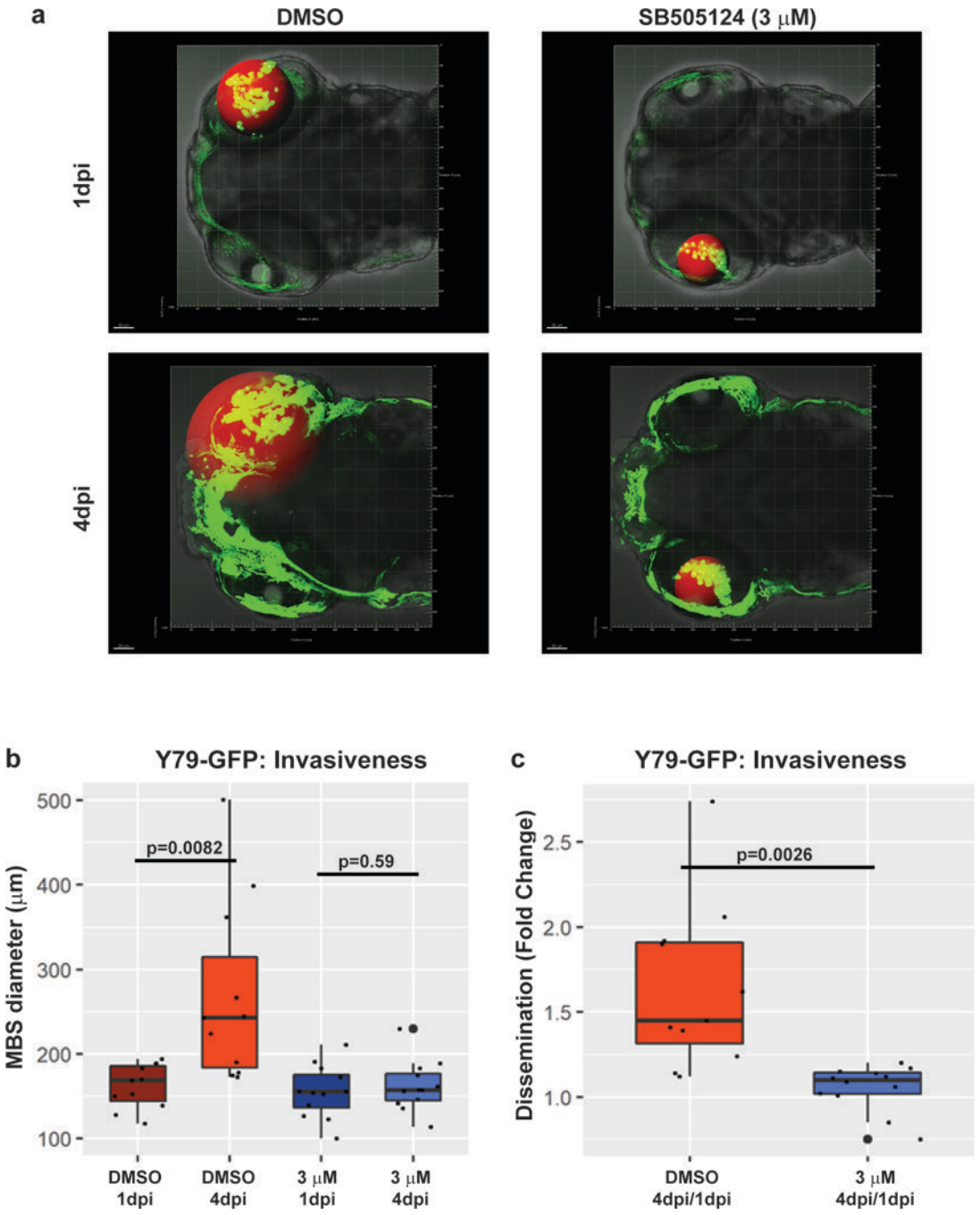

Figure 6. Treatment with SB505124 inhibits cell dissemination in zebrafish embryos.

a: Representative images of the localization of the Y79-GFP cells (green dots), as they were monitored by confocal intravital microscopy at 1 and 4 days post-injection (dpi). The red sphere represents the minimum bounding sphere (MBS), indicative of the dissemination of the cells outside the injection point (50 μm grid for scale). The diffuse green autofluorescence, more evident at 4 dpi, is due to the endogenous iridophore pigmentation of the zebrafish, which was accounted for during the MBS analysis. **b:** The MBS diameter (μm) was significantly increased from day 1 to day 4 when zebrafish larvae (n=12) were

treated with DMSO for 4 days, upon injection of Y79-GFP cells in the vitreous cavity, as opposed to treatment with SB505124 (3 μM), which did not produce any significant increase in the MBS diameter. Effect size for DMSO treatment: 106.91; 95% confidence interval (CI): 33.64, 179.99; p=0.0082; effect size for SB505124 treatment: 6.75; 95% CI:−18.96, 32.46; p=0.59. **c**: 55% reduction in the fold-change of the MBS diameter at 4dpi/1dpi was observed when larvae were treated with 3 μM of SB505124 compared to DMSO. Effect size: −0.57; 95% CI: −0.91, −0.25; p=0.0026. The extent of retinoblastoma dissemination, represented by the MBS diameter, was determined using IMARIS & Matlab software. 50 μm grid for scale.

Table 1.

Genes upregulated in invasive compared to non-invasive retinoblastomas; Fold Change (FC =INV/NON INV) > 2; Log2 FC > 1; probability of differential expression > 0.7.

Gene	P diff. exp.	Log2 FC	Mean NON INV.	Mean INV.	#1	#2	#3	#4	#5	#6	#7	#8	#9	#10
					Non Invasive					Invasive				
ADCYAP1	1	5.833	0.2	28	0	0	0	1	0	1	0	48	0	91
PLGLB2	1	5.538	0.108	25.452	0.05	0.14	0.04	0.17	0.14	0.06	0.09	0.14	126.89	0.08
TBR1	0.998	4.956	1	36.6	1	0	3	0	1	0	1	40	0	142
TPH1	0.998	4.834	69.2	2021.2	10	46	139	68	83	125	68	8358.2	33	1522.1
DLX6	0.995	4.737	0.2	13.6	0	0	1	0	0	0	2	37	0	29
RBM46	0.994	4.735	0.6	24.8	1	1	0	1	0	0	120	0	2	2
CYP19A1	0.994	4.526	0.8	29	1	2	0	1	0	0	0	140	1	4
PRDM12	0.925	4.399	0.2	9.4	0	0	1	0	0	1	0	0	1	45
NMUR2	0.971	4.376	1	23.2	1	1	3	0	0	0	0	2	0	114
SPINK5	0.99	4.26	1.2	32.4	1	3	0	1	1	2	1	149	3	7
MSH4	0.998	3.95	2	37.556	1	1	3	5	0	67	85	31.78	1	3
NPY2R	0.955	3.846	0.4	10.4	0	0	2	0	0	1	3	31	4	13
TFF1	0.947	3.825	10.2	155.2	0	0	0	49	2	4	0	748	1	23
VCX	0.947	3.787	1.544	27.644	0	2.51	3.94	1.27	0	2.24	1.04	131.63	3.31	0
ST6GALNAC5	0.938	3.779	0.6	12	0	1	0	2	0	1	1	28	1	29
GLRA1	0.892	3.741	4.2	50.8	0	6	13	0	2	5	7	19	3	220
GUCY1B2	0.85	3.728	0.2	8	1	0	0	0	0	1	0	39	0	0
GLDN	0.846	3.351	1.2	18	4	1	0	1	0	0	0	90	0	0
KCNA4	0.89	3.32	11.6	122.2	5	5	23	10	15	42	19	444	8	98
CHRNA1	0.729	3.309	3.4	4.6	2	7	1	3	4	12	1	2	8	0
MMP12	0.796	3.278	1.8	18.002	0	0	3	1	5	1	23.01	7	3	56
FAM72D	0.71	3.14	5.1	47.71	0	0	14.08	12.59	0	24.91	41.2	4.92	91.38	78.52
POU4F1	0.814	2.731	2.9	21.25	5	2	3	1	3	18	7	20	8	49
CAMKV	0.707	2.023	9.79	40.89	3	5	10	2	29	79	17	44	75	15
KCNS3	0.985	1.789	8.05	28.69	8	6	16	3	7	18	29	45	25	30

Gene	P diff. exp.	Log2 FC	Mean NON INV.	Mean INV.	Non Invasive					Invasive				
					#1	#2	#3	#4	#5	#6	#7	#8	#9	#10
ACVR1C/ALK7	0.814	1.539	4.24	13	3	5	2	5	6	10	19	18	10	10
NPNT	0.759	1.21	158.34	366.76	242	46	278	33	176	415.45	376	449.32	567.99	175
HIST1H3I	0.984	1.188	17.53	40.4	12	11	24	24	17	53	23	43	44	48
MTMR8	0.909	1.058	12.42	26.24	16	9	15	10	11	23	30	20	36	27
MND1	0.992	1.046	51.5	106.72	61	20	70	33	70	119	83.01	151	117	93
ARHGAP11B	0.927	1.023	87.32	177.77	83.65	44.8	87.93	98.71	117.97	175.01	172.41	243.75	141.63	184.26
CAMK4	0.818	1.01	99.16	200	126	57	107	33	162	200	198.99	183	231	221
IQGAP3	0.905	1.002	88.38	177.39	54	41	120	79	149	184.99	120	221	233.44	175

Oncogene. Author manuscript; available in PMC 2019 May 06.

Table 2.

Genes downregulated in invasive compared to non-invasive retinoblastomas; Fold Change (FC = INV/NON INV) < 0.5; Log2 FC < −1; probability of differential expression > 0.7.

Gene	P diff. exp.	Log2 FC	Mean NON INV.	Mean INV.	#1	#2	#3	#4	#5	#6	#7	#8	#9	#10
					Non Invasive					Invasive				
CRABP1	1	−5.214	141.6	3.8	7	662	1	35	3	10	2	4	0	3
GFAP	0.998	−4.904	2545.296	95	86	12456.48	131	21	32	39	26	335	67	8
NGFR	0.999	−4.884	51.6	1.6	2	247	4	4	1	2	0	2	3	1
DACT2	0.995	−4.844	14.4	0.2	4	65	0	3	0	1	0	0	0	0
SLN	0.996	−4.838	14.8	0.2	0	69	0	5	0	0	0	1	0	0
CLRN1	0.998	−4.757	31.566	1	7	145.83	0	5	0	2	0	1	2	0
ABLIM3	0.999	−4.747	132.928	4.8	14	605.64	16	23	6	0	4	10	5	5
SOX8	0.993	−4.626	13.4	0.2	1	60	0	5	1	0	1	0	0	0
USH1C	0.999	−4.601	33.8	1	3	145	0	21	0	0	0	1	1	3
OAF	0.998	−4.571	66.4	2.6	6	304	0	22	0	1	3	4	3	2
VSX2	0.997	−4.501	48.686	2.004	5	233.43	0	5	0	6	1.02	0	1	2
MOXD1	0.997	−4.492	30.6	1	6	145	0	2	0	2	0	0	0	3
TF	0.988	−4.383	5094.2	244.708	445	23201.03	231.97	1556	37	125	159.54	84	357	498
HKDC1	0.997	−4.382	69.8	3.2	3	307	1	38	0	7	3	3	0	3
PRPH	0.984	−4.371	17	0.6	1	84	0	0	0	0	0	0	3	0
WIF1	0.991	−4.333	559.14	29.858	52	2681.7	6	53	3	18	9	22	67.29	33
OR4F17	0.996	−4.288	23.2	0.7	22	431	3	13	4	12	5	0	7	2
CRYM	0.993	−4.269	10.25	13.968	4	8.82	14.8	14	9.63	10	12.01	13.15	26.55	8.13
RHO	0.993	−4.255	1445.604	1742.364	1605.95	1665	1406.02	1290	1261.05	1587.91	1853.03	1680	1924	1666.88
LOC644172	0.986	−4.244	11.2	0.2	7	0	0	47	2	0	0	0	0	1
CDC42EP1	0.976	−4.189	12.4	0.4	1	53	4	3	1	1	0	1	0	0
SAG	0.998	−4.186	49.19	2.37	50	177	4	5	0	2	0	1	1	7
COL22A1	0.985	−4.171	19.29	0.74	0	83	0	11	1	0	0	4	0	0
NDP	0.988	−4.156	29.13	1.3	7	128	1	3	3	0	1	1	4	1
ITGB4	0.987	−4.124	110.67	6.01	2	517	8	7	8	5	7	13	8	0

Gene	P diff. exp.	Log2 FC	Mean NON INV.	Mean INV.	#1	#2	#3	#4	#5	#6	#7	#8	#9	#10
					Non Invasive					Invasive				
IGJ	0.995	−4.071	118.03	6.68	2	572	2	0	1	0	9	0	0	20
ELK2AP	0.99	−4.032	73.63	4.16	0	358	0	0	2	0	20	0	0	0
IGLL5	0.982	−4.006	465.13	28.61	13	2252.06	4	0	4	0	122.66	4	4	7
CLU	0.922	−4.002	3125.32	194.68	309	14302.14	397	174.01	107	88	135	438	296	92
GNAT1	0.995	−3.989	124.3	7.49	72	432	8.07	80	14	13	0	5	12	10
NFIX	0.98	−3.984	236.84	14.64	24	1033.81	39	57	8	7	8	28	27	9
CPA6	0.983	−3.922	18.21	0.86	6	73	0	10	0	0	3	0	0	1
OLR1	0.98	−3.907	24.54	1.3	1	117.94	1	0	0	0	2	0	1	3
CRYAA	0.961	−3.863	153.86	10.25	9	738.6	3	1	0	6	5	3	33	9
TRDN	0.979	−3.855	265.04	17.99	17	1241.22	0	35	3	8	0	25	6	46
GPX6	0.961	−3.788	206.29	14.6	3	6	3	1060	0	1	0	67	4	6
TBX5	0.96	−3.743	23.79	1.45	3	97	1	15	1	3	1	0	3	1
TBX3	0.922	−3.733	13.74	0.7	4	59	1	3	0	0	0	2	2	0
CYP4F11	0.964	−3.725	20.61	1.23	3	89	0	9	0	0	2	0	2	2
MAOB	0.97	−3.661	131.12	10.03	20	580	5	22	14	0	6	18	4	20
TMX2-CTNND1	0.992	−3.659	53.79	3.93	50.62	0	78.15	0	137.5	23.56	0	0	0	0
LIX1	0.958	−3.658	209.77	16.29	56	896.25	25.98	39	7	6	10	25	17	24.03
MYZAP	0.946	−3.653	16.17	0.96	6.21	65.75	5.69	1.26	0	0	0	1.85	1.42	1.59
MIR31HG	0.758	−3.634	6.12	0.17	0	29	0	1	0	0	0	0	1	0
FGFRL1	0.956	−3.611	53.39	4.04	0	231	5	27	0	2	3	7	5	4
C3	0.947	−3.609	271.32	21.91	15	1294	13	1	3	0	33	29	2	39
ABCC3	0.941	−3.59	27.56	1.96	1	126	2	3	3	0	1	6	1	2
GABRR3	0.939	−3.548	12.47	0.74	2	39.03	0	21	0	3	0	0	0	1
CHRNA9	0.89	−3.547	6.71	0.24	4	0	0	25	5	0	0	0	0	1
PAPPA2	0.924	−3.526	149.33	12.63	16	688	7	17	2	7	7	12	18	20
PSD4	0.875	−3.52	9.98	0.54	2	38	3	2	4	1	1	0	1	0
DKK3	0.841	−3.486	1257.23	111.92	336	5341.01	139.1	252.96	70	52	131	93	114	166
LOC645434	0.803	−3.482	5.48	0.17	2	17	3	3	2	0	0	0	1	0

Gene	P diff. exp.	Log2 FC	Mean NON INV.	Mean INV.	#1	#2	#3	#4	#5	#6	#7	#8	#9	#10
					Non Invasive					Invasive				
PKP1	0.967	−3.478	19.68	1.44	3	76	0	18	0	0	0	0	0	6
KIAA0125	0.837	−3.476	8.59	0.45	0	42	0	0	0	0	1	0	0	1
HLA-DRB6	0.943	−3.436	36.53	3.05	0	42	0	0	0	0	1	0	0	1
BOC	0.869	−3.435	14.53	1.02	1	63.52	1.14	5.69	0	1.1	0	2.16	1.14	1.04
SYNPR	0.958	−3.422	27.53	2.24	13	109	0	12	0	1	1	1	0	7
NPY1R	0.936	−3.415	19.17	1.47	3	0	9	87.27	0	0	2	0	2	3
TLL2	0.973	−3.402	11.23	0.74	10	10	4	30	2	1	0	0	2	1
LOC101929555	0.829	−3.401	11.39	0.76	0	51	4	0	1	0	0	1	2	1
C4B	0.87	−3.393	122.68	11.36	0	563.33	18.43	11.48	8.71	8.15	8.2	24.65	10.76	8.19
GOLGA8M	0.98	−3.389	27.42	2.29	1.26	43.36	85.79	5.19	4.83	3.04	0	0	2.13	5.95
NAV2	0.971	−3.362	371.22	35.79	46	921.06	53	837.25	7	20	18	37	48	57.9
LEFTY2	0.892	−3.354	24.78	2.1	5	103	1	1	11	0	3	4	3	1
FCGR2C	0.917	−3.333	39.57	3.61	1.14	181.55	2	1	8	0	3.95	3	2.18	7.78
SERPING1	0.757	−3.308	530.06	53.22	58	2438.9	45	28	21	12	59	115	26	56
SLC24A3	0.821	−3.305	7.95	0.48	1	33	1	2	2	0	0	0	0	2
CFB	0.858	−3.28	76.37	7.54	5	345	10	4	10	0	7	21	5	5.8
LTBR	0.78	−3.277	8.69	0.57	0	34	7	0	2	0	0	0	2	1
PTPRQ	0.836	−3.269	10.03	0.72	1	46	0	1	1	0	0	0	0	3
HEPN1	0.844	−3.263	40.98	3.95	7	172.29	9.24	10	2.4	3.8	0.44	9.65	5.82	2
ARHGEF37	0.873	−3.256	41.63	4.04	1	191	1	7	4	1	7	7	1	4
ESPN	0.861	−3.251	16.28	1.39	1	55	3	21	1	4	1	1	2	0
RGL3	0.771	−3.25	14.65	1.22	1	62.02	1	7	1	1	0	3	3	0
SIGLEC1	0.757	−3.25	16.3	1.39	0	74	3	1	2	2	1	1	4	0
CHI3L1	0.875	−3.242	244.81	25.56	32	1047.54	6	104	11	0	40	18	10	51
FAM69C	0.795	−3.242	37.42	3.64	2	176.01	1	3	1	2	1	11	5	1
RRH	0.869	−3.241	57.64	5.77	8	254	4	10	6	6	8	1	6	8
LEPREL1	0.85	−3.232	70.82	7.22	15	310.03	4	17	0	3	9.99	3	13	8
GPR37	0.844	−3.203	88.25	9.26	34.93	80.57	46.26	58.52	35.48	44.6	28.32	46.67	46.1	17.83

Oncogene. Author manuscript; available in PMC 2019 May 06.

Gene	P diff. exp.	Log2 FC	Mean NON INV.	Mean INV.	#1	#2	#3	#4	#5	#6	#7	#8	#9	#10
					Non Invasive					Invasive				
NOTCH1	0.901	−3.176	78.3	8.35	4	253	14	106	13	5	3	24	12	2
COL23A1	0.802	−3.166	12.42	1.06	0	55	1	3	2	0	2	0	1	2
VAV1	0.709	−3.165	7.14	0.48	0	34	1	0	0	0	0	0	0	2
PTGDS	0.806	−3.158	104.09	11.34	9	453	20	26	3	2	11	24	10	11
KIAA1217	0.764	−3.152	235.85	26.21	40	976	27	95	19	24	16	23	36	36
PAX6	0.764	−3.147	282.61	31.59	51	1229	15	67	20	39	35	10	15	56
FAM189A2	0.788	−3.132	25.15	2.55	2	117	1	3	0	3	4	0	3	3
PPP1R1B	0.725	−3.12	9.81	0.81	1	42	0	1	4	1	0	0	1	2
RLBP1	0.825	−3.104	158.99	18.17	24	702	2	50	0	6	42	0	3	33
G6PC2	0.818	−3.091	15.9	1.55	1	71	1	5	0	0	0	1	1	5
DDX11L1	0.795	−3.082	7.64	0.58	0	26.57	0	6.82	4.44	0	0	0	0	2.43
PLXNB3	0.762	−3.07	11.16	1.02	1	44.02	3	5	2	1	0	2	0	2
GSTM5	0.742	−3.067	14.67	1.44	0	68.92	0	3	0	0	3	0	2	2
CYP21A1P	0.715	−3.067	17.82	1.81	0	72.45	5.69	3	6.7	3.56	0	5.7	1	0
COL4A5	0.822	−3.063	26.41	2.85	6	99	7	16	2	2	4	2	5	2
AGT	0.774	−3.035	15.88	1.62	8	63	0	1	5	0	3	1	2	2
MYL9	0.731	−3.01	15.6	1.63	3	58	7	9	0	3	0	3	2	1
ADAMTS19	0.844	−3.004	15.4	1.61	2	59	0	15	0	0	0	0	1	6
KLKB1	0.752	−2.997	45.41	5.37	3	200.01	1	16.8	2	7	3	5	3	9
CLIC5	0.823	−2.991	58.77	7.08	3	248	3	26	9	5	7	2	2	17
TICAM2	0.832	−2.984	17.58	1.91	41.74	13.32	24	0	4.48	11.46	0	0	0	0
B3GAT1	0.839	−2.978	27.1	3.13	8	86	4	33	3	1	2	8	5	1
LRP10	0.755	−2.973	49.81	6.03	11	202	8	14	9	4	7	12	3	5
LOC100126784	0.72	−2.972	14	1.47	1	55.98	6	6.14	0	2	0	2	1	2.52
NPVF	0.786	−2.962	184.18	23.32	10	806.7	0	88	0	14	3	0	1	84
UNC5B	0.809	−2.906	59.21	7.59	6	196	14	71.26	7	7	1	17	7	8
FGF13	0.911	−2.872	19.92	2.41	5	43	2	50	0	0	2	3	0	6
UST	0.718	−2.869	24.31	3.02	5.36	98	7.99	8	0	1	2	4	3	5

Oncogene. Author manuscript; available in PMC 2019 May 06.

Gene	P diff. exp.	Log2 FC	Mean NON INV.	Mean INV.	#1	#2	#3	#4	#5	#6	#7	#8	#9	#10
					Non Invasive					Invasive				
CYP2J2	0.709	−2.844	8.93	0.93	2	32	0	9	1	0	1	0	0	3
MGARP	0.745	−2.836	37.71	4.98	6	158.86	1	16	3	3	4	1	2	13
LINC01002	0.9	−2.818	14.53	1.75	0	14.69	13.97	5.45	39.05	0	0	1.59	3.32	3.77
FAM43A	0.721	−2.623	17.75	2.57	4	26	8	51	1	1	2	5	5	1
FOXP2	0.738	−2.568	53.31	8.69	11	162	0	91	1	1	4	1	9	25
NXF2	0.791	−2.431	14.17	2.34	0	17.05	24.5	22.5	8.5	6	0	4	0	2.5
NXF2B	0.791	−2.431	14.17	2.34	16.01	34.78	27.84	22.12	23.24	17.85	2.21	3.18	7.35	2.51
AKR1C2	1	−2.026	24.92	5.85	16.01	34.78	27.84	22.12	23.24	17.85	2.21	3.18	7.35	2.51
HERC2P3	0.889	−1.357	121.46	47.2	149.55	115.56	158.61	125.71	49.04	95	47.86	34.55	36.32	37.41
ACTA2	0.789	−1.27	43	17.62	52	64	38	30	26	15	22	22	13	18
ADPGK-AS1	0.874	−1.073	20.82	9.71	16.36	17	25.61	28	17	4	10	14	9	12